Biochimica et Biophysica Acta 1798 (2010) 2048–2057

Contents lists available at ScienceDirect

Biochimica et Biophysica Acta

journal homepage: www.elsevier.com/locate/bbamem

Claudin-3 acts as a sealing component of the tight junction for ions of either charge and uncharged solutes

Susanne Milatz [a], Susanne M. Krug [a], Rita Rosenthal [a], Dorothee Günzel [a], Dominik Müller [b], Jörg-Dieter Schulzke [c], Salah Amasheh [a,1], Michael Fromm [a,*,1]

[a] Institute of Clinical Physiology, Charité, Campus Benjamin Franklin, Berlin, Germany
[b] Department of Pediatric Nephrology, Charité, Campus Virchow-Klinikum, Berlin, Germany
[c] Department of General Medicine, Charité, Campus Benjamin Franklin, Berlin, Germany

ARTICLE INFO

Article history:
Received 11 March 2010
Received in revised form 2 July 2010
Accepted 16 July 2010
Available online 22 July 2010

Keywords:
MDCK II cells
Epithelial barrier
Transepithelial resistance
Permeability
Freeze fracture EM
Impedance spectroscopy

ABSTRACT

The paracellular barrier of epithelia and endothelia is established by several tight junction proteins including claudin-3. Although claudin-3 is present in many epithelia including skin, lung, kidney, and intestine and in endothelia, its function is unresolved as yet. We therefore characterized claudin-3 by stable transfection of MDCK II kidney tubule cells with human claudin-3 cDNA. Two clone systems were analyzed, exhibiting high or low claudin-2 expression, respectively. Expression of other claudins was unchanged. Ultrastructurally, tight junction strands were changed toward uninterrupted and rounded meshwork loops. Functionally, the paracellular resistance of claudin-3-transfected monolayers was strongly elevated, causing an increase in transepithelial resistance compared to vector controls. Permeabilities for mono- and divalent cations and for anions were decreased. In the high-claudin-2 system, claudin-3 reduced claudin-2-induced cation selectivity, while in the low-claudin-2 system no charge preference was observed, the latter thus reflecting the "intrinsic" action of claudin-3. Furthermore, the passage of the paracellular tracers fluorescein (332 Da) and FD-4 (4 kDa) was decreased, whereas the permeability to water was not affected. We demonstrate that claudin-3 alters the tight junction meshwork and seals the paracellular pathway against the passage of small ions of either charge and uncharged solutes. Thus, in a kidney model epithelium, claudin-3 acts as a general barrier-forming protein.

1. Introduction

Tight junctions (TJs) are the apical-most components of borders between adjacent cells, regulating the passage of ions and solutes via the paracellular pathway. Four types of transmembranal proteins located within the TJ have been identified: junctional adhesion molecule (JAM) [1], occludin [2], tricellulin [3], and the group of claudins [4]. The claudin family represents the main component of TJ strands, creating an ion-selective border between apical and basolateral compartments. To date, 24 mammalian claudins have been discovered. Several claudins have been shown to strengthen the paracellular barrier, e.g. claudin-1 [5], claudin-4 [6], claudin-5 [7,8], and claudin-8 [9–11]. On the other hand, some claudins exhibit properties of selective pores, e.g. claudin-2 [12,13], claudin-10a and claudin-10b [14,15]. While most claudins show a highly tissue-specific expression pattern, claudin-3 is a ubiquitous TJ protein, expressed in epithelia of intestine, kidney, liver, skin, lung, and in endothelia. In the blood–brain barrier (BBB), it is assumed to be a central component determining the integrity of the TJ [16]. Due to its omnipresence in different tissues and organs, it appears as a part of the basic equipment of TJ strands.

Claudin-3, formerly named rat ventral prostate protein 1 (RVP1), became generally known as functional receptor for the *Clostridium perfringens* enterotoxin (CPE) [17–20]. In numerous studies, it has been shown to be regulated during tumor genesis in various organs and tissues, e.g. in breast [21,22], ovaries [23–27], uterus [28], prostate [29], and esophagus [30].

Thus, claudin-3 is considered as an emerging target for cancer detection and therapy [31,32], although its functional role in cancer progression is unknown as yet [33], last not least because of its unclear role in barrier formation.

Within tubular structures like intestine and nephron, claudin-3 has been shown to be expressed stronger in distal than in proximal segments [34,35]. Recently, it has been shown that expression of claudin-3 along segments of rat intestine correlates with barrier properties measured by means of impedance spectroscopy [36]. Considering the distinct barrier function of these tissues, a tightening role of claudin-3 can be cautiously assumed. This concept is supported by previous studies: Coyne et al. transfected mouse fibroblast cells

* Corresponding author. Institute of Clinical Physiology, Charité, Campus Benjamin Franklin, Hindenburgdamm 30, 12203 Berlin, Germany.
E-mail address: michael.fromm@charite.de (M. Fromm).
[1] Equally contributing.

0005-2736/$ – see front matter © 2010 Elsevier B.V. All rights reserved.
doi:10.1016/j.bbamem.2010.07.014

(NIH/3T3) and the human airway epithelial cell line IB3.1 with human claudin-3 cDNA and observed a trend toward an increase in transepithelial resistance which did not, however, reach significance in either cell line. Overexpression of claudin-3 in NIH/3T3 cells had no effect on permeability to 10, 70, and 2000 kDa dextrans, while overexpression in IB3.1 cells caused a decrease of permeability [37]. Moreover, knockdown of claudin-3 resulted in a marginal (−16%) or a marked (−70%) decrease of R^t in Madin–Darby canine kidney (MDCK) II cells, or human gastric adenocarcinoma cells (MKN28), respectively [38,39].

Taken together, previous studies imply a sealing effect of claudin-3, although its precise function is experimentally unsolved. In order to obtain deeper insights into the function of claudin-3, we overexpressed human claudin-3 in MDCK cells, subclone II, which represents a well established cell line with paracellular characteristics resembling the proximal nephron. To this end, we demonstrate that claudin-3 acts as a sealing component of the TJ for mono- and divalent ions and for molecules of 332 Da and 4 kDa.

2. Materials and methods

2.1. Cell culture

Madin–Darby canine kidney cells, subclone II (MDCK II) were grown in culture flasks containing MEM (PAA Laboratories, Pasching, Austria), supplemented with 10% fetal bovine serum (Biochrom, Berlin, Germany) and 1% penicillin/streptomycin (PAA Laboratories). Cells were cultured at 37 °C in a humidified 5% CO_2 atmosphere. For all experiments, with the exception of transfection and co-immunoprecipitation, cells were grown on permeable polycarbonate culture plate inserts (Millicell HA, 0.6 cm², pore size 0.45 μm Millipore, Bedford, MA, USA).

2.2. Stable transfection

Human claudin-3 cDNA was obtained by isolation of total RNA from the human colon carcinoma cell line Caco-2, followed by reverse transcription and specific amplification by means of polymerase chain reaction (PCR). After verification of the PCR product by DNA sequence analysis, it was inserted into the eukaryotic expression vector pFLAG-CMV-10 (Sigma Aldrich, Taufkirchen, Germany). MDCK II cells were stably transfected with the pFLAG-CMV-10-claudin-3 construct, further referred to as pFLAG-CLD3, employing Lipofectamine Plus™ reagent (Invitrogen, Carlsbad, CA, USA). In parallel, another set of cells was transfected with the empty vector to serve as control. Transfected cells were treated with the antibiotic G418 (PAA Laboratories, Pasching, Austria) to select stably transfected clones, containing either pFLAG-CLD3 or the empty vector, respectively. All clones were screened for expression of claudin-3 and other claudins by Western blot analysis.

2.3. Western blotting

Cells were scraped from culture plate inserts and homogenized in lysis buffer (20 mM TRIS, 5 mM $MgCl_2$, 1 mM EDTA, 0.3 mM EGTA) containing protease inhibitors (Complete, Boehringer, Mannheim, Germany). Membrane fractions were obtained by passing through a 26 G × 3/8" needle, followed by a centrifugation at 200*g* for 5 min and subsequent centrifugation of the remaining supernatant at 43,000*g* for 30 min. Extracted protein was diluted in lysis buffer and quantified using the BCA Protein assay reagent (Pierce, Rockford, IL, USA) and a plate reader (Tecan, Grödig, Austria). Aliquots of protein were mixed with sodium dodecyl sulfate (SDS) containing buffer (Laemmli), denatured at 95 °C for 5 min, fractionated on SDS polyacrylamide gels and subsequently blotted onto PVDF membranes (PerkinElmer, Boston, MA, USA). Proteins were detected using specific antibodies against TJ proteins (Invitrogen, Carlsbad, CA, USA) or the FLAG sequence (Sigma Aldrich, Taufkirchen, Germany) respectively, and visualized by luminescence imaging (LAS-1000, Fujifilm, Tokyo, Japan). Signals were quantified by densitometry employing the AIDA application (Raytest, Straubenhardt, Germany).

For Triton X-100 (TX-100) fractionation, cells were homogenized in ice-cold extraction buffer (150 mM NaCl, 15 mM Tris–HCl, pH 7.5, 1 mM $MgCl_2$, 1 mM $CaCl_2$) containing 0.5% TX-100. Cells were incubated on ice for 20 min and subsequently centrifuged at 15,000*g* for 15 min to separate TX-100-soluble from -insoluble material. The TX-100-insoluble pellet was resuspended in an equal volume of extraction buffer. Both fractions were sonicated for 3 × 10 s at an amplitude of 40%. Protein quantification, blotting, detection, and visualization were performed as described above.

2.4. Co-immunoprecipitation

Cells were scraped from flasks and homogenized in lysis buffer (150 mM NaCl, 25 mM TRIS, 5 mM EDTA, 0.1% SDS, 1% Nonidet P40, 1% sodium deoxycholate) containing protease inhibitors (Complete, Boehringer, Mannheim, Germany). Whole cell lysates were obtained by centrifugation at 15,000*g* for 15 min. 250 μg of total protein was mixed with 4 μg antibody and incubated over night at 4 °C. Protein A agarose beads (Upstate, Lake Placid, NY, USA) were washed with lysis buffer and incubated with the protein/ antibody mixture for 1 h. Agarose beads were isolated by centrifugation (1000*g*; 1 min), washed with lysis buffer and denatured in Laemmli buffer at 95 °C for 20 min. Beads were pelleted (14,000*g*) and supernatant was fractionated on SDS polyacrylamide gels. Protein blotting, detection and visualization were performed as already described.

2.5. Immunofluorescence microscopy

Cells were grown to confluence on permeable culture plate inserts and fixed with absolute ethanol for 10 min at −20 °C. After permeabilization with phosphate-buffered saline (PBS) containing 0.5% Triton X-100 for 7 min, cell layers were preincubated with a blocking solution (PBS containing 5% goat serum) for 15 min at room temperature to avoid unspecific binding. For subsequent immunostaining of TJ proteins, cells were incubated for 60 min with specific antibodies, diluted 1:100 (anti-claudin and anti-occludin antibodies) or 1:600 (anti-FLAG antibody) in blocking solution. After washing, cell layers were exposed to secondary antibodies (Alexa Fluor goat anti-rabbit IgG or Alexa Fluor goat anti-mouse IgG with wavelengths of 488 or 594 nm, Molecular Probes, USA, diluted 1:500 in blocking solution) for 60 min. Nuclei were stained with 4',6-diamidino-2-phenylindole (DAPI, 461 nm, diluted 1:1,000 in blocking solution). Finally, cells were mounted onto microscope slides in ProTags MountFluor (Biocyc, Luckenwalde, Germany) and fluorescence images were obtained with a confocal laser-scanning microscope (Zeiss LSM 510 Meta, Zeiss, Germany).

2.6. Freeze fracture electron microscopy

Cells grown on permeable culture plate inserts were fixed with phosphate-buffered 2.5% glutaraldehyde and equilibrated in 10% and 30% glycerol. After freezing in liquid nitrogen-cooled Freon 22, preparations were fractured at −100 °C and shadowed with platinum and carbon in a vacuum evaporator (Denton DV-502, Cherry Hill, NJ, USA). Replicas were bleached with sodium hypochloride, picked up on grids (Ted Pella Inc., Tustin, CA, USA), and examined with a video-equipped Zeiss 902 electron microscope (Carl Zeiss AG, Oberkochen, Germany; Olympus iTEM Veleta, Münster, Germany). TJs were morphometrically analyzed at a final magnification of 51,000×. Perpendicular to the most apical TJ strand, vertical grid lines were layered at 200-nm intervals [40]. The number of horizontally oriented

TJ strands was counted at intersections with grid lines. The distance between the most apical and contra-apical strand was measured as the compact meshwork depth. Strand discontinuities within the compact TJ meshwork of >20 nm were defined as "breaks." Strand formation was noted as "particle type" or "continuous type." Finally, the predominance of "rounded mesh loops" or "angular mesh loops" was counted.

2.7. Two-path impedance spectroscopy

All electrophysiological analyses were performed on confluent cell monolayers grown on culture plate inserts which were mounted in Ussing chambers. Two-path impedance spectroscopy was performed as recently described [41]. Briefly, the epithelial resistance (R^{epi}) consisting of two parallel resistors, the paracellular resistance (R^{para}), caused by the barrier properties of the TJ, and the transcellular resistance (R^{trans}), determined by the cell membranes, is in series to the subepithelial resistance (R^{sub}) which is caused by the filter support. In this equivalent circuit the apical and the basolateral membranes of the confluent cell layer are represented by resistors and capacitors in parallel adding up to R^{trans} and C^{trans}. After application of alternating current (35 μA/cm^2, frequency range 1.3 Hz to 65 kHz), voltage changes were detected by a phase-sensitive amplifier (402 frequency response analyzer, Beran Instruments, Glen Allen, VA, USA; 1286 electrochemical interface; Solartron Schlumberger, Atlanta, GA, USA). Complex impedance loci (Z^{real}, $Z^{imaginary}$) were calculated and plotted in a Nyquist diagram. R^{trans} and R^{para} were determined from experiments in which impedance spectra and fluxes of the paracellular marker substance fluorescein were obtained before and after chelating extracellular Ca^{2+} with EGTA. This caused TJs to partly open and to increase fluorescein flux inversely proportional to R^{epi} changes. The justification of this procedure was assessed in separate experiments (data not shown).

2.8. Measurement of ion permeabilities

Measurement of ion permeabilities was performed as described in detail elsewhere [15]. All measurements were carried out in circulating Ringer's solution, gassed with O_2 or 95% O_2 / 5% CO_2 at a temperature of 37 °C and a pH of 7.4.

For dilution potential measurements, the chamber system filled with 10 ml Ringer's solution (21 mM $NaHCO_3$, 119 mM NaCl, 5.4 mM KCl, 1 mM $MgSO_4$, 1.2 mM $CaCl_2$, 3 mM HEPES, 10 mM glucose) on each side. pH was maintained by constant equilibration with 95% O_2/5% CO_2. After acclimatization of cells, 5 ml of the basolateral or apical bathing solution were replaced by a modified Ringer's solution containing 238 mM mannitol instead of 119 mM NaCl. Transepithelial resistance and voltage were recorded during the whole experiment, and permeability ratios for Na^+ and Cl^- (P_{Na}/P_{Cl}) were calculated according to the Goldman-Hodgkin-Katz equation. Permeabilities for K^+, Li^+, Rb^+, and Cs^+ were investigated by replacing 5 ml of the standard bathing solution by a modified Ringer's solution containing the particular ion instead of Na^+. For measurement of bi-ionic potentials of divalent cations (Ca^{2+}, Mg^{2+}, Sr^{2+}, Ba^{2+}) and anions other than Cl^-, experiments were carried out in a similar manner. Standard Ringer's solution contained 140 mM NaCl, 5.4 mM KCl, 1 mM $MgCl_2$, 1.2 mM $CaCl_2$, 10 mM HEPES, and 10 mM glucose and cells were gassed with O_2.

Absolute permeabilities were calculated from relative permeabilities and transepithelial resistances as described elsewhere [15].

2.9. Fluxes of paracellular tracers

Measurements of unidirectional tracer fluxes from the apical to the basolateral side were performed by the use of fluorescein and fluorescein isothiocyanate (FITC)-labelled dextran (4 kDa). In fluorescein flux studies, samples were taken every 10 min after addition of the tracer molecule for a period of 40 min. In experiments with FITC-dextran, four 30 min flux periods were analyzed. Fluorescein and FITC-dextran concentrations were measured with a fluorometer at 520 nm (Spectramax Gemini, Molecular devices, Sunnyvale, CA, USA).

2.10. Measurement of water permeability

Water permeability was measured as recently described [42]. Briefly, confluent cells, seeded on cell culture inserts, were mounted into modified Ussing chambers with glass tubes instead of gas lifts and maintained in HEPES buffered Ringer's solution. Water passage was induced by generation of a transepithelial osmotic gradient with mannitol (100 mM). The fluid level in both chamber tubes was monitored by a video optic system ColorView XS (Olympus Soft Imaging Solutions GmbH), at time 0 min and every 15 min over a period of 2 hours. Water flux (J) was determined from the difference between the menisci at the registration times and permeability P was calculated from $P = J/\Delta c$ ($\Delta c = 100$ mmol/l).

2.11. Statistical analysis

Values are reported as mean ± standard error of the mean with n as the number of experiments. Statistical analysis was performed using the unpaired, two-tailed Student's *t* test, except for categorial data (lower 2 lines of Table 1), where Fisher's exact test was applied. $p<0.05$ was considered significant.

3. Results

3.1. Stable expression of human claudin-3 in MDCK II cells

MDCK II is a leaky cell line, characterized by a low paracellular resistance which is mainly caused by the conductive properties of claudin-2. In this cell line, claudin-3 is only weakly expressed. To analyze the contribution of claudin-3 to paracellular barrier properties, we stably transfected MDCK II cells with human claudin-3 cDNA, carrying a 3xFLAG tag at its 5' end. Cells transfected with the empty plasmid served as controls. Stable transfection with claudin-3 cDNA led to a strong expression of human claudin-3, tagged by 3xFLAG at the N-terminus of the protein (Fig. 1A). Analysis of immunofluorescent micrographs revealed a distinct increase of claudin-3 within the TJ, shown by colocalization with the TJ marker occludin. Because the employed first antibody was able to bind both, the canine and the human form of claudin-3, the correct localization of exogenous claudin-3 was verified by staining of the 3×FLAG peptide (Fig. 2A).

Exogenous claudin-3 expression did not alter the expression levels or localization of the TJ proteins occludin, claudin-1, claudin-4, claudin-7, or claudin-8 (Fig. 1A). In contrast, expression of claudin-2 strongly differed among claudin-3-transfected clones. The majority of claudin-3-overexpressing clones showed a marked reduction of

Table 1
Morphometric analysis of freeze fracture electron microscopy.

	VEC-1	CLD3-1	VEC-2	CLD3-2
n tissues/grids	11/28	11/18	15/16	12/34
Number of horizontal strands	4.3 ± 0.2	4.5 ± 0.3	4.8 ± 0.3	4.9 ± 0.3
Compact meshwork depth (nm)	246 ± 17	371 ± 41**	332 ± 37	429 ± 38
Density of strands (1/pm)	17.5 ± 1.6	12.1 ± 1.6*	14.3 ± 1.9	11.5 ± 1.3
Breaks per μm single strand	1.6 ± 0.1	0.1 ± 0.1**	0.2 ± 0.1	0.3 ± 0.1
Particle type: continuous type	5 : 6	0 : 11*	5 : 10	0 : 12*
Angular type : curved type	11 : 0	1 : 10***	15 :0	2 : 10***

*$p<0.05$, **$p<0.01$, *** $p<0.001$ versus respective vector controls.

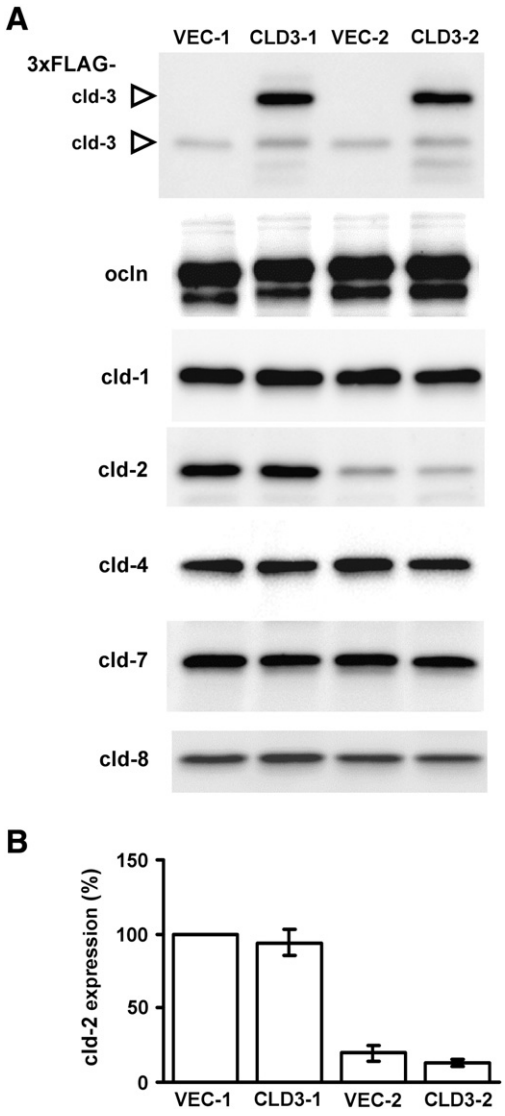

Fig. 1. Expression of tight junction proteins in claudin-3-transfected cells and respective vector controls. (A) Expression of claudin-3 (cld-3), occludin (ocln), and claudin (cld) −1, −2, −4, −7, −8. Upper bands on the claudin-3 blot indicate exogenous 3xFLAG tagged claudin-3, lower bands endogenous expression. (B) Densitometric analysis of claudin-2 expression in high-claudin-2 (VEC-1, CLD3-1) and low-claudin-2 (VEC-2, CLD3-2) systems; expression of VEC-1, which represents typical MDCK II cells, was set 100%; $n = 3$.

claudin-2 or acquired claudin-2 depletion during passaging, as visualized by immunostaining (Fig. 2A). Among vector controls, most clones displayed typically high claudin-2 expression, although we also detected clones with reduced claudin-2 levels.

Thus we employed two clone systems, exhibiting "high" or "low" claudin-2 expression: First, we selected one vector control (VEC-1) and two claudin-3-overexpressing clones (CLD3-1a and CLD3-1b) with high claudin-2 expression as typically found in MDCK II cells. Moreover, we selected two vector controls (VEC-2a, VEC-2b) and two claudin-3-transfected clones (CLD3-2a, CLD3-2b) with low claudin-2 expression levels that were reduced to about 16 % (Fig. 1B). In order to provide information on the distribution of claudin-2 within the actin-based TJ pool and the cytosolic pool that is not associated with the TJ, we analyzed claudin-2 content in the TX-100-soluble and -insoluble protein pools and observed no alteration of TJ-associated claudin-2 in CLD3-1 compared to VEC-1 or in CLD3-2 compared to VEC-2 ($101.0 \pm 1.5\%$ or $86.9 \pm 18.4\%$ versus vector controls, respectively; Fig. 2B).

The effects of claudin-3 overexpression were analyzed in both, the high and low claudin-2 system. Claudin-3 expression did not differ among all employed claudin-3-transfected clones.

If not stated otherwise, experiments were carried out on two selected clones of each CLD3-1, VEC-2, and CLD3-2 and results of one exemplary clone are shown. We employed only one clone of VEC-1 because this clone resembles normal MDCK II cells which are already well characterized.

3.2. Altered tight junction meshwork by claudin-3 overexpression

In both clone systems, with high or with low claudin-2 expression, transfection with claudin-3 led to an alteration of the TJ meshwork pattern. Vector controls showed a morphology of predominantly angled loops as typically found in MDCK II cells. In contrast, claudin-3-transfected cells exhibited a pattern of curved strands with the formation of large, rounded mesh loops (Fig. 3, Table 1). As a result, the depth of the compact meshwork was increased and the strand density reduced in the CLD3-1 clone, while congruent changes in the CLD3-2 clone did not reach statistical significance. The total number of horizontal strands remained unchanged in both claudin-3-overexpressing clones (Table 1, Fig. 4).

VEC-1 and VEC-2 differed in frequency of strand breaks: Whereas VEC-1 with high claudin-2 presence showed 1.6 ± 0.1 breaks per µm strand, the number of strand breaks was 0.2 ± 0.1 in VEC-2 with low claudin-2. Overexpression of claudin-3 in clone system 1 led to a strong reduction of strand breaks to 0.1 ± 0.1. In clone system 2, claudin-3 transfection had no further influence on the already low number of strand breaks (CLD3-2: 0.3 ± 0.1 per µm). Particle type strands were noted in 5 of 11 VEC-1 tissues and in 5 of 15 VEC-2 tissues. In both claudin-3 overexpressing clones, the number of particle type strands was reduced to zero. Most noteworthy, in both systems claudin-3 overexpression caused a complete disappearance of particle-typed strands in favor of a continuous strand pattern (Table 1).

3.3. Dramatic increase of paracellular resistance

To analyze the specific effect of claudin-3 overexpression on TJ-related resistance, we employed two-path-impedance spectroscopy which allows measuring paracellular (R^{para}) and transcellular resistances (R^{trans}) as two parallel components of epithelial resistance (R^{epi}). In controls, R^{para} and R^{epi} were higher in VEC-2 than in VEC-1, reflecting the low-claudin-2 expression of system 2 (Fig. 5).

In the high-claudin-2 cells of system 1, R^{epi} increased from $22 \pm 3\ \Omega{\cdot}cm^2$ in VEC-1 to $79 \pm 3\ \Omega{\cdot}cm^2$ in CLD3-1. This increase was based on a dramatic increase of R^{para} from $37 \pm 6\ \Omega{\cdot}cm^2$ in VEC-1 to $549 \pm 66\ \Omega{\cdot}cm^2$ in CLD3-1, a 15-fold change. R^{trans} was not significantly changed ($76 \pm 17\ \Omega{\cdot}cm^2$ in VEC-1 versus $50 \pm 26\ \Omega{\cdot}cm^2$ in CLD3-1), indicating no alteration of conductive membrane channels or carriers.

Along similar lines, in the low-claudin-2 cells of system 2, R^{epi} increased from $44 \pm 4\ \Omega{\cdot}cm^2$ in VEC-2 to $113 \pm 6\ \Omega{\cdot}cm^2$ in CLD3-2. Again, this increase was based on a strong increase of R^{para} from $105 \pm 18\ \Omega{\cdot}cm^2$ in VEC-2 to $935 \pm 225\ \Omega{\cdot}cm^2$ in CLD3-2, a 9-fold change. Also here, R^{trans} was not significantly changed ($110 \pm 16\ \Omega{\cdot}cm^2$ in VEC-2 versus $132 \pm 9\ \Omega{\cdot}cm^2$ in CLD3-2), indicating no alteration of conductive membrane channels or carriers.

3.4. Claudin-3 seals against cations and anions

Elevation of R^{para} may be caused by preferred sealing against cations, anions, or both. In order to determine single ion permeabilities, we measured dilution potentials. In cells with high claudin-2 level, overexpression of claudin-3 led to a marked decrease in sodium permeability from $37.0 \pm 0.8 \times 10^{-6}$ cm/s (VEC-1) to $14.2 \pm 0.4 \times 10^{-6}$ cm/s (CLD3-1), whereas the permeability of chloride was

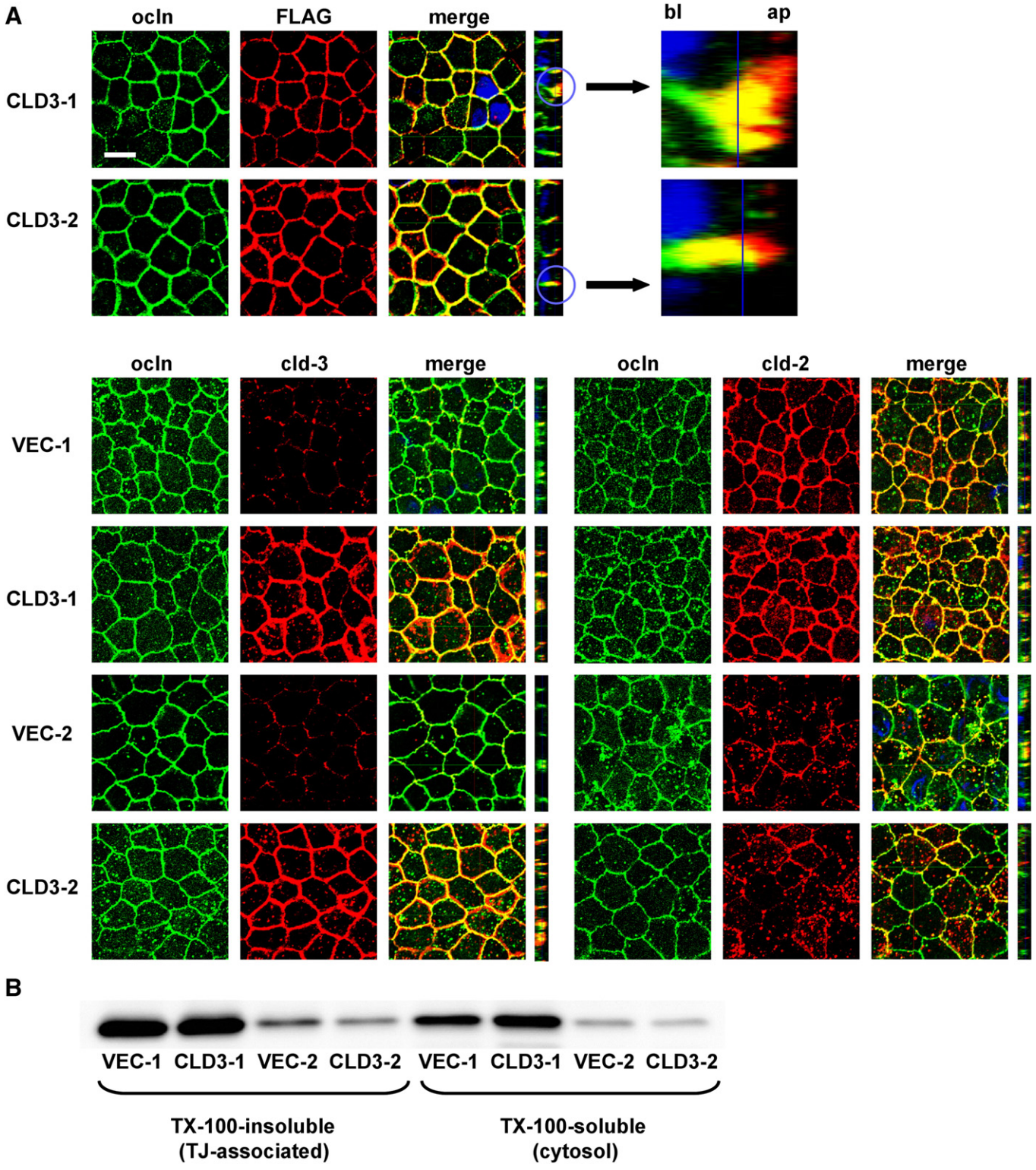

Fig. 2. Subcellular localization and distribution of TJ proteins in claudin-3-transfected cells and vector controls. (A) Immunofluorescent microscopy. FLAG, claudin-3 (cld-3), or claudin-2 (cld-2) were colocalized with the tight junction marker occludin (ocln). MDCK II cells express low levels of claudin-3, correct localization of exogenous claudin-3 is indicated by staining of FLAG. Bar indicates 10 μm. Y-z sections provide a lateral view on the TJ which is localized at the apical cell pole (ap) whereas DAPI stained nuclei (blue) reside more basally (bl). (B) Distribution of claudin-2 in TX-100-soluble and -insoluble protein fractions. TJ-associated claudin-2 was not altered in claudin-3-overexpressing cells of both clone systems compared to respective vector controls; $n = 3$.

less affected ($11.2 \pm 0.8 \times 10^{-6}$ cm/s in VEC-1 vs. $8.0 \pm 0.4 \times 10^{-6}$ cm/s in CLD3-1; Fig. 6A). The ratio P_{Na}/P_{Cl} was decreased from 3.4 ± 0.2 (VEC-1) to 1.8 ± 0.1 (CLD3-1), indicating a decrease in cation selectivity (Fig. 6B). In contrast, in low-claudin-2 vector controls, sodium permeability was relatively low (VEC-2: $18.6 \pm 1.1 \times 10^{-6}$ cm/s), whereas the permeability to chloride was similar to that of VEC-1

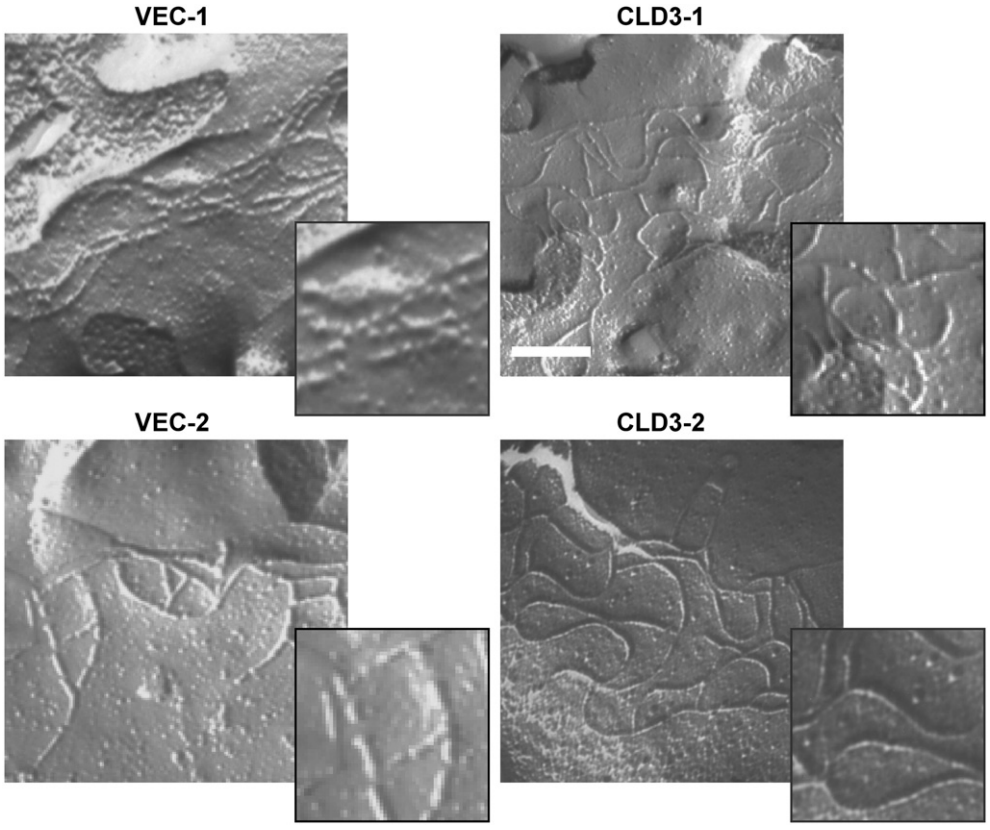

Fig. 3. Freeze fracture electron micrographs of vector controls and claudin-3-overexpressing cells. Claudin-3 transfection led to an alteration of tight junction meshwork pattern by formation of continuous strands with rounded loops. Bar indicates 200 nm.

(VEC-2: $11.3 \pm 0.8 \times 10^{-6}$ cm/s). Claudin-3 overexpression resulted in decreased permeabilities to both, sodium (CLD3-2: $9.6 \pm 0.7 \times 10^{-6}$ cm/s) and chloride (CLD3-2: $6.5 \pm 0.7 \times 10^{-6}$ cm/s). The ratio P_{Na}/P_{Cl} in VEC-2 was relatively low (1.7 ± 0.1), due to low claudin-2 expression, and was not altered by claudin-3-transfection (1.6 ± 0.1 in CLD3-2). Thus, claudin-3-mediated alteration in charge selectivity depends on endogenous claudin-2 expression.

3.5. Eisenman sequences: no alteration in ion sorting

Bi-ionic potential measurements of VEC-1, CLD3-1a, VEC-2a and CLD3-2a revealed that claudin-3 overexpression caused a decrease in permeabilities to the alkali metal cations lithium, potassium, rubidium, and cesium that was proportional to the decrease in sodium permeability (Fig. 7A). Despite reduced permeabilities for all tested monovalent cations, overexpression of claudin-3 did not alter the sorting of ions according to the Eisenman sequence [43,44], sealing against all monovalent cations in equal measure. All tested clones followed the Eisenman sequence IX ($Na^+ > K^+ > Li^+ > Rb^+ > Cs^+$), indicating a sorting depending rather on the unhydrated ion radius than on the hydrated ion radius.

To analyze the conductance of divalent cations, we employed VEC-1, CLD3-1a, VEC-2a and CLD3-2a for bi-ionic potential measurements. In both clone systems, claudin-3 overexpression led to decreased permeabilities for magnesium, calcium, strontium, and

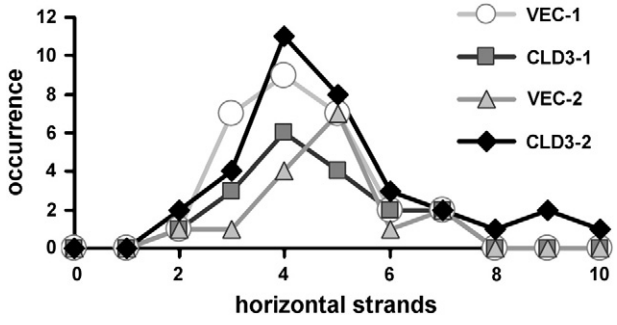

Fig. 4. Frequency distribution of horizontal tight junction strands in vector controls and claudin-3-overexpressing cells, analyzed by freeze fracture electron microscopy. Strand number followed standardized normal distribution in all clones and was not different in controls and claudin-3 overexpressing cells.

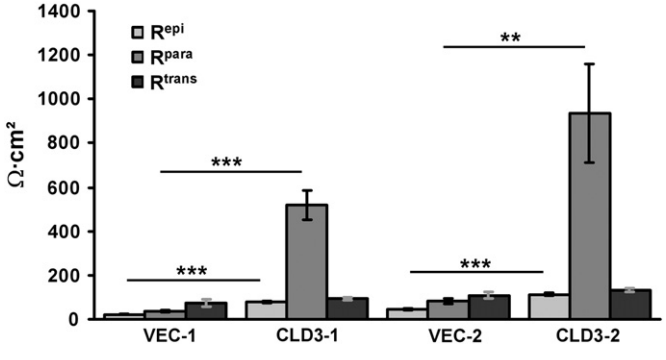

Fig. 5. Results of two-path impedance spectroscopy. Claudin-3 overexpression increased epithelial resistances (R^{epi}), based on strongly elevated paracellular resistances (R^{para}). Transcellular resistances (R^{trans}) were not significantly changed versus respective controls. Claudin-3 overexpression converted an MDCK II leaky epithelium ($R^{para} < R^{trans}$) into a tight epithelium ($R^{para} > R^{trans}$). $^{**}p < 0.01$; $^{***}p < 0.001$; $n = 4$–6.

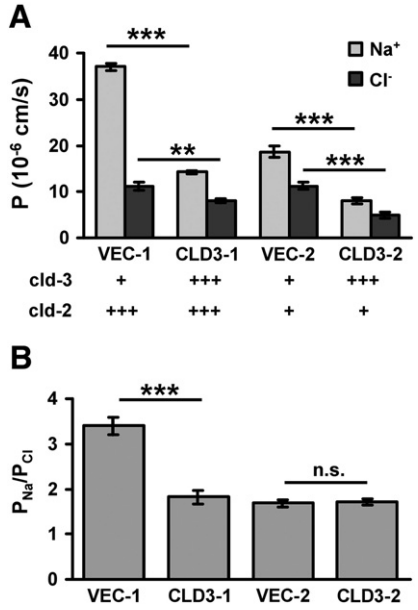

Fig. 6. Permeabilities to Na^+ and Cl^- (A) and P_{Na}/P_{Cl} (B) in clones with different claudin-2 (cld-2) and claudin-3 (cld-3) expression levels as indicated by crosses. In high-claudin-2 vector controls, claudin-3 overexpression caused a decrease in cation selectivity. In low-claudin-2 cells, claudin-3 overexpression decreased permeabilities without alteration of P_{Na}/P_{Cl}. $^{**}p<0.01$; $^{***}p<0.001$; n.s.: $p>0.05$; $n=8$.

barium, compared to vector control (Fig. 7B). The low-claudin-2 vector control, VEC-2, displayed permeabilities to magnesium, calcium, strontium and barium similar to these of VEC-1. Compared with other clones, CLD3-2 showed lowest permeabilities to Mg^{2+}, Ca^{2+}, Sr^{2+}, and Ba^{2+}. All clones exhibited only indistinct ranking of particular divalent cations. Vector controls followed approximately sequence I, II, or III for divalent cations (Ba^{2+}~Sr^{2+}~Ca^{2+}>Mg^{2+}), establishing a paracellular pathway, which sorts depending solely on the hydrated ion radius of divalent cations, but not on their unhydrated ion radius. In claudin-3-expressing cells, no ranking of divalent cation permeabilities was detectable.

To test whether sealing properties of claudin-3-overexpression extended to negatively charged ions other than chloride, we measured permeabilities to fluoride, bromide, and iodide. The permeability to chloride was measured again under the same conditions. Claudin-3 overexpression led to a decrease in permeabilities to all halide anions that was proportional to the decrease in chloride permeability (Fig. 7C). Ranking of anions in vector controls approximated sequence VII for halide anions (F^->Cl^->Br^->I^-), suggesting a strong site that prefers the ion with the smallest nonhydrated radius. In claudin-3-transfected cells, no clear ranking of halogens was detectable.

The results indicate that in MDCK II cells monovalent ions pass the TJ only partially hydrated or unhydrated, irrespective of their charge, whereas divalent cations keep their hydration shell during the paracellular passage.

3.6. Decrease in passage of larger molecules

For further analysis of sealing properties of claudin-3, permeabilities to the marker solute fluorescein (332 Da) and to the macromolecule FD-4 (FITC dextran, 4 kDa) were measured. In all clones, the TJ was less permeable to fluorescein than to smaller cations or anions, and least permeable to FD-4. Different claudin-2 expression levels had no influence on permeabilities of either molecule. Overexpression of claudin-3 caused a decrease in permeability values to fluorescein (VEC-1: 2.3 ± 0.5; CLD3-1: 1.6 ± 0.3; VEC-2: 2.4 ± 0.3; CLD3-2: $1.5\pm0.1\times10^{-6}$ cm/s, Fig. 8A), which did not reach significance in the high-claudin-2 system. Permeabilities to FD-4 were decreased by more than half in both systems (VEC-1: 0.12 ± 0.02; CLD3-1: 0.05 ± 0.004; VEC-2: 0.12 ± 0.04; CLD3-2: $0.035\pm0.008\times10^{-6}$ cm/s, Fig. 8B). Altogether, results indicate a sealing effect of claudin-3 against the tested paracellular marker molecules.

3.7. No influence of claudin-3 on water permeability

To analyze the role of claudin-3 in water transport, we measured osmotically driven water flux in vector controls (VEC-1, VEC-2a) and claudin-3 overexpressing cells (CLD3-1a, CLD3-2a). The low-claudin-2 system generally exhibited slightly lower permeabilities to water than cells with high claudin-2 expression (VEC-1: 8.6 ± 0.3; CLD3-1: 8.5 ± 0.7; VEC-2: 7.1 ± 0.5; CLD3-2: $7.8\pm0.3\times10^{-3}$ cm/s, Fig. 9A). Claudin-3 overexpression did not alter water permeability in either system.

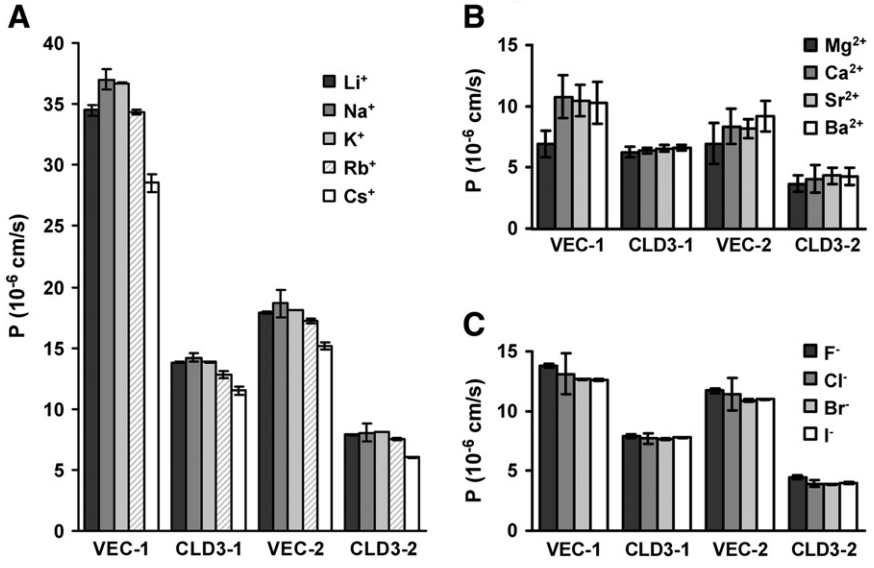

Fig. 7. Permeabilities to alkali cations (A), alkaline-earth cations (B), and halide anions (C) in vector controls and claudin-3-overexpressing clones. Overexpression of claudin-3 led to decreased permeabilities to all sorts of ions without alteration of ion ranking; $n=3$–8.

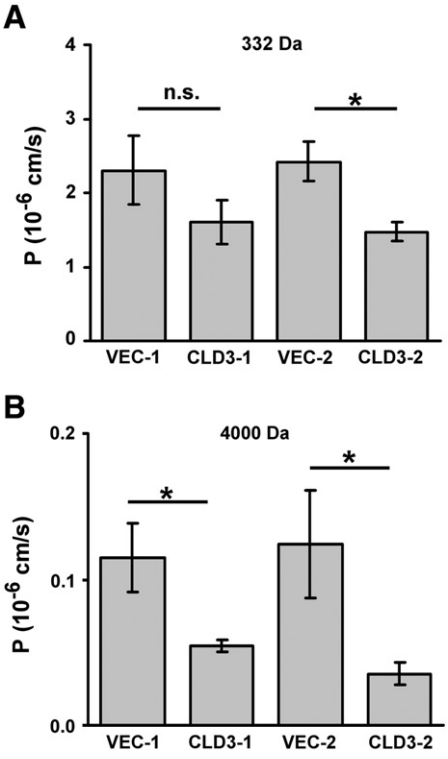

Fig. 8. Permeabilities to fluorescein (332 Da, A) and FD-4 (4 kDa, B). Overexpression of claudin-3 reduced permeabilities to fluorescein and FD-4. $^*p<0.05$, n.s.: $p>0.05$; $n=5$–9.

3.8. Interaction of human claudin-3 and canine claudin-2

To investigate whether or not the differences of claudin-3 overexpression in cell systems with high or low claudin-2 expression could be explained by an interaction of human claudin-3 and canine claudin-2. Therefore, co-immunoprecipitation using antibodies to FLAG or claudin-3 and subsequent immunoblotting with anti-claudin-2 antibody was performed in cells with strong expression of both proteins (CLD3-1). As shown in Fig. 9B, interaction of exogenous claudin-3 and endogenous claudin-2 took place.

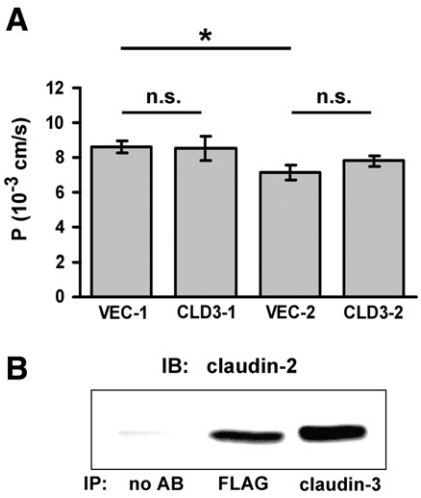

Fig. 9. Permeability to water and co-immunoprecipitation of claudin-3 and claudin-2. (A) Water permeability in vector controls and claudin-3-overexpressing cells is shown. $^*p<0.05$, n.s.: $p>0.05$; $n=9$. (B) Co-immunoprecipitation of claudin-3 and claudin-2: Whole cell lysates of clone CLD3-1 were immunoprecipitated using antibodies to FLAG or claudin-3. Lysates without antibody (no AB) served as control. Co-immunoprecipitation with endogenous claudin-2 was determined by immunoblot.

4. Discussion

4.1. Implications of altered tight junction ultrastructure

The most striking effect of claudin-3 overexpression on TJ ultrastructure was the almost complete change from a pattern of angular type meshwork loops to curved type loops. This has been previously observed when claudin-3 was expressed in fibroblasts [37,45]. Since claudin-3 is able to form autonomous strands with the typical curved appearance and its overexpression did not alter the expression of other claudins within the same clone system, it is likely that the characteristic loops are dominated by claudin-3. Interestingly, a very similar morphology has been reported in claudin-4-overexpressing MDCK II cells [6], however it remains unsolved whether or not curved strands affect paracellular permeability.

Claudin-3 overexpression did not cause a change in the number of horizontally oriented strands but markedly reduced the number of strand breaks and led to a complete disappearance of discontinuous "particle type" strands. The occurrence of strand breaks and the presence of "particle type" strands in VEC-1 are characteristic for claudin-2-expressing cells [45]. Both features disappeared upon claudin-3 overexpression (CLD3-1).

In the low-claudin-2 VEC-2, strand breaks were almost absent and claudin-3 expression (CLD3-2) had no further effect. Thus, the number of strand breaks did not correlate with permeability changes within this second system. Even more importantly, breaks in both systems were too rare to contribute significantly to paracellular permeability [46] and in no case did they open a complete vertical pathway across the TJ meshwork.

The complete disappearance of particle type strands in favor of continuous type strands in both clone systems correlates well with the observed permeability changes, but it is unknown yet whether this is an epiphenomenon of altered TJ protein composition or has a causal effect. Concerning the appearance of strand breaks and particle type strands, claudin-2 and claudin-3 seem to act in an antagonistic way.

4.2. Sole paracellular effect on transepithelial resistance

Former studies had suggested a rather tightening role of claudin-3, as they observed a tendency toward an increased R^t in claudin-3-overexpressing cells and decreased R^t values in cells treated with claudin-3 siRNA [37–39]. In accordance with these findings, overexpression of human claudin-3 in the low-resistance cell line MDCK II caused a two- to threefold increase in R^{epi}. However, by two-path impedance spectroscopy we were able to discriminate between para- and transcellular components of R^{epi} and found that the basis of this transepithelial effect was a 9- to 15-fold increase in R^{para}, which was not accompanied by any change in R^{trans}. Thus, Claudin-3 expression in MDCK II cells converted this leaky epithelium ($R^{para}<R^{trans}$) into a tight epithelium ($R^{para}>R^{trans}$). This result clearly indicates a pronounced barrier effect of claudin-3.

4.3. Possible mechanisms of claudin-3 sealing effect

Overexpression of claudin-3 caused a marked reduction of the paracellular permeability to inorganic cations and anions, fluorescein, and FD-4. MDCK II cells are characterized by a high, claudin-2-mediated cation selectivity and a cation ion preference according to Eisenman sequence IX, even in the low-claudin-2 clone. The fact that claudin-3 decreased the permeability to monovalent cations without alteration of this Eisenman sequence indicates that TJ properties in claudin-3-overexpressing cells were still governed by claudin-2-based channels, although their number or single-channel permeability was reduced.

In cell system 2 (low claudin-2 expression), claudin-3 decreased permeabilities to inorganic cations and anions, fluorescein, and FD-4 in almost equal measure (~50% of control). This might be due to a "rarefaction effect" on paracellular pores for ions and solutes, caused by additional insertion of exogenous claudin-3 in TJ strands, as indicated by the characteristic strand bending.

In cell system 1 (high claudin-2 expression) the effect on cation permeability was disproportionately strong, implying a specific effect on cation selectivity of the host cell system. A similar phenomenon was described by Van Itallie et al. [6,47], who reported different effects of claudin-4 overexpression on charge preference in cation-selective MDCK II and slightly anion-selective LLC-PK_1 cells.

A likely explanation for our findings is that claudin-3 generally seals the TJ equally to cations and anions. In strongly cation selective cells the disproportionate effect of claudin-3 on cation permeability might be due to an increased probability for a direct *cis*- or *trans*-interaction between claudins 2 and 3. Such interactions have previously been shown for mouse claudin-2 und -3 [45], and were confirmed for human claudin-3 and canine claudin-2 in the present study. It is hypothesized that this interaction leads to a preferential loss of cation-pores.

4.4. Water permeability

It has been a longstanding discussion whether or not water is able to pass the TJ and if so, to which extent claudins take part in this process. Recently, we have shown that claudin-2 acts as a paracellular water channel [42]. In accordance with this finding, water permeability in MDCK II vector controls with low claudin-2 expression was lower than in cells with high claudin-2. Assuming a direct correlation between claudin-2 expression and paracellular water permeability, it can be estimated that the paracellular water permeability in the low-claudin-2 system was reduced to approximately 20%. The relatively small effect on total water permeability (reduction to 87% in clone system 2) is explained by the strong expression of aquaporins mediating transcellular water flux in MDCK II cells.

The finding that claudin-3 overexpression in the low-claudin-2 system reduced the number of claudin-2-based pores without affecting water permeability appears to be contradictory. It was beyond the scope of the present study to resolve the mechanistic basis of this finding. However, it is our working hypothesis that purely claudin-2- and hybrid claudin-2/claudin-3-based paracellular channels differ with regard to their functional properties. In high-claudin-2 vector controls TJ properties are determined mainly by the formation of "pure" claudin-2-based pores, allowing the passage of cations and water. After claudin-3-transfection, TJ formation is predominated by combined expression and interaction of claudin-2 and claudin-3. These claudin-2/claudin-3 hybrid pores may still be water-permeable, but with critically reduced charge density within the pore. This would reduce cation permeability while water permeation was retained. Further investigation is needed to analyze the properties of claudin-2/claudin-3-based TJs concerning the paracellular water permeability.

4.5. Relation between claudin-3 and claudin-4

Claudin-3 is a ubiquitously expressed TJ protein and assumed to be part of the standard equipment of junctional strands like claudin-1 or claudin-4. Nevertheless, there are subtle distinctions in expression patterns [34,35]. Especially in endothelial TJs of the blood–brain barrier, claudin-3 seems to play a crucial role [16]. Functionally, claudin-3 resembles claudin-4 in several ways: both claudins seal the TJ against the passage of ions, thereby increasing R^t and are able to restrict the paracellular passage of macromolecules [37,48].

On ultrastructural level, overexpression of claudin-3 or claudin-4 led to very similar strand patterns with formation of curved loops, whereas claudin-1 or claudin-5 overexpression did not [6,37]. The observed similarities between claudin-3 and claudin-4 may be explained by a high sequence homology and their genomic neighborhood on human chromosome 7, suggesting evolutionary gene duplication. In fact, 67% of amino acids are identical, the extracellular loops 1 and 2 have 94% and 68% of amino acids in common, respectively. Whereas barrier or pore properties of claudins are determined by their extracellular loops, the strand morphology seems to depend upon other domains [49]. Although claudin-3 and claudin-4 are often commonly expressed and transcriptionally regulated [23,50,51], there seem to be differences in regulatory pathways on protein level, e.g. phosphorylation [52]. This is due to the non-homologous C-termini, which are supposed to be crucial for intracellular signaling.

Claudin-3 and -4 also differ in their capability of interacting with other claudins. Whereas claudin-3 is capable of heterophilic *trans*-interactions with claudin-1, -2, and -5 *trans*-interactions of claudin-4 with other claudins could not be demonstrated [37,45,53].

4.6. General barrier function of claudin-3

The initial idea for studying two systems with different claudin-2 expression levels was that system 1, with its high claudin-2 expression, represented the unaltered and well established cell line MDCK II. However, it appeared that claudin-2 and claudin-3 may significantly interact, so that the effect of claudin-3 could not be separated. System 2 exhibited low claudin-2 expression and thus allowed to study the "pure" effect of claudin-3.

As our main finding we prove that claudin-3 acts as a barrier-forming TJ component that strongly reduces the paracellular permeability to ions and to larger uncharged solutes but not to osmotically driven water. In addition, we demonstrate that claudin-3 barrier properties depend on the expression level of claudin-2, which acts as an opponent player in barrier formation. If the effect of the cation channel claudin-2 is suppressed, the "intrinsic" action of claudin-3 is uncovered and turned out to be without ion charge preference, while in the presence of claudin-2 it reduces cation permeability more than that for anions. In conclusion, in a kidney model epithelium claudin-3 acts as a general barrier-forming protein.

Acknowledgments

Supported by DFG Forschergruppe FOR 721, by DFG GU 447/11-1, and by Sonnenfeld-Stiftung, Berlin.

References

[1] I. Martin-Padura, S. Lostaglio, M. Schneemann, L. Williams, M. Romano, P. Fruscella, C. Panzeri, A. Stoppacciaro, L. Ruco, A. Villa, D. Simmons, E. Dejana, Junctional adhesion molecule, a novel member of the immunoglobulin superfamily that distributes at intercellular junctions and modulates monocyte transmigration, J. Cell Biol. 142 (1998) 117–127.
[2] M. Furuse, T. Hirase, M. Itoh, A. Nagafuchi, S. Yonemura, S. Tsukita, S. Tsukita, Occludin: a novel integral membrane protein localizing at tight junctions, J. Cell Biol. 123 (1993) 1777–1788.
[3] J. Ikenouchi, M. Furuse, K. Furuse, H. Sasaki, S. Tsukita, S. Tsukita, Tricellulin constitutes a novel barrier at tricellular contacts of epithelial cells, J. Cell Biol. 171 (2005) 939–945.
[4] M. Furuse, H. Sasaki, K. Fujimoto, S. Tsukita, A single gene product, claudin-1 or -2, reconstitutes tight junction strands and recruits occludin in fibroblasts, J. Cell Biol. 143 (1998) 391–401.
[5] M. Furuse, M. Hata, K. Furuse, Y. Yoshida, A. Haratake, Y. Sugitani, T. Noda, A. Kubo, S. Tsukita, Claudin-based tight junctions are crucial for the mammalian epidermal barrier: a lesson from claudin-1-deficient mice, J. Cell Biol. 156 (2002) 1099–1111.
[6] C.M. Van Itallie, C. Rahner, J.M. Anderson, Regulated expression of claudin-4 decreases paracellular conductance through a selective decrease in sodium permeability, J. Clin. Invest. 107 (2001) 1319–1327.
[7] T. Nitta, M. Hata, S. Gotoh, Y. Seo, H. Sasaki, N. Hashimoto, M. Furuse, S. Tsukita, Size-selective loosening of the blood-brain barrier in claudin-5-deficient mice, J. Cell Biol. 161 (2003) 653–660.
[8] S. Amasheh, T. Schmidt, M. Mahn, P. Florian, J. Mankertz, S. Tavalali, A.H. Gitter, J.D. Schulzke, M. Fromm, Contribution of claudin-5 to barrier properties in tight junctions of epithelial cells, Cell Tissue Res. 321 (2005) 89–96.

[9] A.S.L. Yu, A.H. Enck, W.I. Lencer, E.E. Schneeberger, Claudin-8 expression in Madin–Darby canine kidney cells augments the paracellular barrier to cation permeation, J. Biol. Chem. 278 (2003) 17350–17359.
[10] S. Angelow, K.J. Kim, A.S. Yu, Claudin-8 modulates paracellular permeability to acidic and basic ions in MDCK II cells, J. Physiol. 571 (2006) 15–26.
[11] S. Angelow, E.E. Schneeberger, A.S. Yu, Claudin-8 expression in renal epithelial cells augments the paracellular barrier by replacing endogenous claudin-2, J. Membr. Biol. 215 (2007) 147–159.
[12] M. Furuse, K. Furuse, H. Sasaki, S. Tsukita, Conversion of zonulae occludentes from tight to leaky strand type by introducing claudin-2 into Madin–Darby canine kidney I cells, J. Cell Biol. 153 (2001) 263–272.
[13] S. Amasheh, N. Meiri, A.H. Gitter, T. Schöneberg, J. Mankertz, J.D. Schulzke, M. Fromm, Claudin-2 expression induces cation-selective channels in tight junctions of epithelial cells, J. Cell Sci. 115 (2002) 4969–4976.
[14] C.M. Van Itallie, S. Rogan, A. Yu, L.S. Vidal, J. Holmes, J.M. Anderson, Two splice variants of claudin-10 in the kidney create paracellular pores with different ion selectivities, Am. J. Physiol. Renal. Physiol. 291 (2006) F1288–F1299.
[15] D. Günzel, M. Stuiver, P.J. Kausalya, L. Haisch, S.M. Krug, R. Rosenthal, I.C. Meij, W. Hunziker, M. Fromm, D. Müller, Claudin-10 exists in six alternatively spliced isoforms that exhibit distinct localization and function, J. Cell Sci. 122 (2009) 1507–1517.
[16] H. Wolburg, K. Wolburg-Buchholz, J. Kraus, G. Rascher-Eggstein, S. Liebner, S. Hamm, F. Duffner, E. Grote, W. Risau, B. Engelhardt, Localization of claudin-3 in tight junctions of the blood–brain barrier is selectively lost during experimental autoimmune encephalomyelitis and human glioblastoma multiforme, Acta Neuropathol. 105 (2003) 586–592.
[17] M.M. Briehl, R.L. Miesfeld, Isolation and characterization of transcripts induced by androgen withdrawal and apoptotic cell death in the rat ventral prostate, Mol. Endocrinol. 5 (1991) 1381–1388.
[18] J. Katahira, N. Inoue, Y. Horiguchi, M. Matsuda, N. Sugimoto, Molecular cloning and functional characterization of the receptor for *Clostridium perfringens* enterotoxin, J. Cell Biol. 136 (1997) 1239–1247.
[19] J. Katahira, H. Sugiyama, N. Inoue, Y. Horiguchi, M. Matsuda, N. Sugimoto, *Clostridium perfringens* enterotoxin utilizes two structurally related membrane proteins as functional receptors in vivo, J. Biol. Chem. 272 (1997) 26652–26658.
[20] K. Morita, M. Furuse, K. Fujimoto, S. Tsukita, Claudin multigene family encoding four-transmembrane domain protein components of tight junction strands, Proc. Natl Acad. Sci. 96 (1999) 511–516.
[21] A.M. Tokes, J. Kulka, S. Paku, A. Szik, C. Paska, P.K. Novak, L. Szilak, A. Kiss, K. Bögi, Z. Schaff, Claudin-1, -3 and -4 proteins and mRNA expression in benign and malignant breast lesions: a research study, Breast Cancer Res. 7 (2005) R296–R305.
[22] S.L. Kominsky, M. Vali, D. Korz, T.G. Gabig, S.A. Weitzman, P. Argani, S. Sukumar, *Clostridium perfringens* enterotoxin elicits rapid and specific cytolysis of breast carcinoma cells mediated through tight junction proteins claudin 3 and 4, Am. J. Pathol. 164 (2004) 1627–1633.
[23] H. Honda, M.J. Pazin, T. D'Souza, H. Ji, P.J. Morin, Regulation of the CLDN3 gene in ovarian cancer cells, Cancer Biol. Ther. 6 (2007) 1733–1742.
[24] C.D. Hough, C.A. Sherman-Baust, E.S. Pizer, F.J. Montz, D.D. Im, N.B. Rosenshein, K.R. Cho, G.J. Riggins, P.J. Morin, Large-scale serial analysis of gene expression reveals genes differentially expressed in ovarian cancer, Cancer Res. 60 (2000) 6281–6287.
[25] K.H. Lu, A.P. Patterson, L. Wang, R.T. Marquez, E.N. Atkinson, K.A. Baggerly, L.R. Ramoth, D.G. Rosen, J. Liu, I. Hellstrom, D. Smith, L. Hartmann, D. Fishman, A. Berchuck, R. Schmandt, R. Whitaker, D.M. Gershenson, G.B. Mills, R.C. Bast Jr, Selection of potential markers for epithelial ovarian cancer with gene expression arrays and recursive descent partition analysis, Clin. Cancer Res. 10 (2004) 3291–3300.
[26] A.D. Santin, F. Zhan, S. Bellone, M. Palmieri, S. Cane, E. Bignotti, S. Anfossi, M. Gokden, D. Dunn, J.J. Roman, T.J. O'Brien, E. Tian, M.J. Cannon, J. Shaughnessy Jr, S. Pecorelli, Gene expression profiles in primary ovarian serous papillary tumors and normal ovarian epithelium: identification of candidate molecular markers for ovarian cancer diagnosis and therapy, Int. J. Cancer 112 (2004) 14–25.
[27] V.A. Heinzelmann-Schwarz, M. Gardiner-Garden, S.M. Henshall, J. Scurry, R.A. Scolyer, M.J. Davies, M. Heinzelmann, L.H. Kalish, A. Bali, J.G. Kench, L.S. Edwards, P.M. Vanden Bergh, N.F. Hacker, R.L. Sutherland, P.M. O'Brien, Overexpression of the cell adhesion molecules DDR1, claudin 3, and Ep-CAM in metaplastic ovarian epithelium and ovarian cancer, Clin. Cancer Res. 10 (2004) 4427–4436.
[28] A.D. Santin, S. Bellone, E.R. Siegel, J.K. McKenney, M. Thomas, J.J. Roman, A. Burnett, G. Tognon, E. Bandiera, Overexpression of *Clostridium perfringens* enterotoxin receptors claudin-3 and claudin-4 in uterine carcinosarcomas, Clin. Cancer Res. 13 (2007) 3339–3346.
[29] H. Long, C.D. Crean, W.H. Lee, O.W. Cummings, T.W. Gabig, Expression of *Clostridium perfringens* enterotoxin receptors claudin-3 and claudin-4 in prostate cancer epithelium, Cancer Res. 61 (2001) 7878–7881.
[30] H. Takala, J. Saarnio, H. Wiik, Y. Soini, Claudins 1, 3, 4, 5 and 7 in esphageal cancer: loss of claudin 3 and 4 expression is associated with metastatic behavior, APMIS 115 (2007) 838–847.
[31] S.L. Kominsky, B. Tyler, J. Sosnowski, K. Brady, M. Doucet, D. Nell, J.G. Smedley, B. McClane, H. Brem, S. Sukumar, *Clostridium perfringens* enterotoxin as a novel-targeted therapeutic for brain metastasis, Cancer Res. 67 (2007) 7977–7982.
[32] Y. Matsuda, S. Semba, J. Ueda, T. Fuku, T. Hasuo, H. Chiba, N. Sawada, Y. Kuroda, H. Yokozak, Gastric and intestinal claudin expression at the invasive front of gastric carcinoma, Cancer Sci. 98 (2007) 1014–1019.
[33] P.J. Morin, Claudin proteins in human cancer: promising new targets for diagnosis and therapy, Cancer Res. 65 (2005) 9603–9606.
[34] C. Rahner, L.L. Mitic, J.M. Anderson, Heterogenity in expression and subcellular localization of claudins 2, 3, 4, and 5 in the rat liver, pancreas, and gut, Gastroenterology 120 (2001) 411–422.
[35] Y. Kiuchi-Saishin, S. Gotoh, M. Furuse, A. Takasuga, Y. Tano, S. Tsukita, Differential expression patterns of claudins, tight junction membrane proteins, in mouse nephron segments, J. Am. Soc. Nephrol. 13 (2002) 875–886.
[36] A.G. Markov, A. Veshnyakova, M. Fromm, M. Amasheh, S. Amasheh, Segmental expression of claudin proteins correlates with tight junction barrier properties in rat intestine, J. Comp. Physiol. B 180 (2010) 591–598.
[37] C.B. Coyne, T.M. Gambling, R.C. Boucher, J.L. Carson, L.G. Johnson, Role of claudin interactions in airway tight junctional permeability, Am. J. Physiol. Lung Cell. Mol. Physiol. 285 (2003) 1166–1178.
[38] J. Hou, A.S. Gomes, D.L. Paul, D.A. Goodenough, Study of claudin function by RNA interference, J. Biol. Chem. 281 (2006) 36117–36123.
[39] K. Hashimoto, T. Oshima, T. Tomita, Y. Kim, T. Matsumoto, T. Joh, H. Miwa, Oxidative stress induces gastric epithelial permeability through claudin-3, Biochem. Biophys. Res. Commun. 376 (2008) 154–157.
[40] B.R. Stevenson, J.M. Anderson, D.A. Goodenough, M.S. Mooseker, Tight junction structure and ZO-1 content are identical in two strains of Madin–Darby canine kidney cells which differ in transepithelial resistance, J. Cell Biol. 107 (1988) 2401–2408.
[41] S.M. Krug, M. Fromm, D. Günzel, Two-path impedance spectroscopy for measuring paracellular and transcellular epithelial resistance, Biophys. J. 97 (2009) 2202–2211.
[42] R. Rosenthal, S. Milatz, S.M. Krug, B. Oelrich, J.D. Schulzke, S. Amasheh, D. Günzel, M. Fromm, Claudin-2, a component of the tight junction, forms a paracellular water channel, J. Cell Sci. 123 (2010) 1913–1921.
[43] G. Eisenman, Cation selective glass electrodes and their mode of operation, Biophys. J. 2 (1962) 259–323.
[44] J.M. Diamond, E.M. Wright, Biological membranes: the physical basis of ion and nonelectrolyte selectivity, Annu. Rev. Physiol. 31 (1996) 581–646.
[45] M. Furuse, H. Sasaki, S. Tsukita, Manner of interaction of heterogeneous claudin species within and between tight junction strands, J. Cell Biol. 147 (1999) 891–903.
[46] S.M. Krug, S. Amasheh, J.F. Richter, S. Milatz, D. Günzel, J.K. Westphal, O. Huber, J.D. Schulzke, M. Fromm, Tricellulin forms a barrier to macromolecules in tricellular tight junctions without affecting ion permeability, Mol. Biol. Cell 20 (2009) 3713–3724.
[47] C.M. Van Itallie, A.S. Fanning, J.M. Anderson, Reversal of charge selectivity in cation or anion-selective epithelial lines by expression of different claudins, Am. J. Physiol. Renal. Physiol. 285 (2003) F1078–F1084.
[48] H. Michikawa, J. Fujita-Yoshigaki, H. Sugiya, Enhancement of barrier function by overexpression of claudin-4 in tight junctions of submandibular gland cells, Cell Tissue Res. 334 (2008) 255–264.
[49] O.R. Colegio, C.M. Van Itallie, C. Rahner, J.M. Anderson, Claudin extracellular domains determine extracellular charge selectivity and resistance but not tight junction fibril architecture, Am. J. Physiol. Cell Physiol. 284 (2003) 1346–1354.
[50] H. Honda, M.J. Pazin, H. Ji, R.P. Wernyj, P.J. Morin, Crucial roles of Sp1 and epigenetic modifications in the regulation of the CLDN4 promoter in ovarian cancer cells, J. Biol. Chem. 281 (2006) 21433–21444.
[51] S. Satake, S. Semba, Y. Matsuda, Y. Usami, H. Chiba, N. Sawada, M. Kasuga, H. Yokozaki, (2008), CDX2 transcription factor regulates claudin-3 and claudin-4 expression during intestinal differentiation of gastric carcinoma, Pathol. Int. 58 (2008) 156–163.
[52] T. D'Souza, R. Agarwal, P.J. Morin, Phosphorylation of claudin-3 at threonine 192 by cAMP-dependent protein kinase regulates tight junction barrier function in ovarian cancer cells, Exp. Cell Res. 280 (2005) 3364–3375.
[53] B.L. Daugherty, C. Ward, T. Smith, J.D. Ritzenthaler, M. Koval, Regulation of heterotypic claudin compatibility, J. Biol. Chem. 282 (2007) 30005–30013.